Proceedings of the ASME 2023 International Technical Conference and Exhibition on Packaging and Integration of Electronic and Photonic Microsystems
InterPACK2023
October 24-26, 2023, San Diego, California

IPACK2023-110576

Thermal, Hydraulic and Reliability Analysis of Single-Phase Liquid Coolants for Direct-to-Chip Cold Plate Cooling in High-Performance Computing Systems

Pardeep Shahi
Nvidia Corporation
Santa Clara, CA

Ali Heydari
Nvidia Corporation
Santa Clara, CA

Chandraprakash Hinge
The University of Texas at Arlington
Arlington, TX

Lochan Sai Reddy Chintaparthy
The University of Texas at Arlington
Arlington, TX

Himanshu Modi
The University of Texas at Arlington
Arlington, TX

Harold Miyamura
Nvidia Corporation
Santa Clara, CA

Mohammad Tradat
Nvidia Corporation
Santa Clara, CA

Uschas Chowdhury
Nvidia Corporation
Santa Clara, CA

Vahideh Radmard
Nvidia Corporation
Santa Clara, CA

Dereje Agonafer
The University of Texas at Arlington
Arlington, TX

Jeremy Rodriguez
Nvidia Corporation
Santa Clara, CA

ABSTRACT

Due to the increasing computational demand driven by artificial intelligence, machine learning, and the Internet of Things (IoT), there has been an unprecedented growth in transistor density for high-end CPUs and GPUs. This growth has resulted in high thermal dissipation power (TDP) and high heat flux, necessitating the adoption of advanced cooling technologies to minimize thermal resistance and optimize cooling efficiency. Among these technologies, direct-to-chip cold plate-based liquid cooling has emerged as a preferred choice in electronics cooling due to its efficiency and cost-effectiveness. In this context, different types of single-phase liquid coolants, such as propylene glycol (PG), ethylene glycol (EG), DI water, treated water, and nanofluids, have been utilized in the market. These coolants, manufactured by different companies, incorporate various inhibitors and chemicals to enhance long-term performance, prevent bio-growth, and provide corrosion resistance. However, the additives used in these coolants can impact their thermal performance, even when the base coolant is the same. This paper aims to compare these coolant types and evaluate the performance of the same coolant from different vendors. The selection of coolants in this study is based on their performance, compatibility with wetted materials, reliability during extended operation, and environmental impact, following the guidelines set by ASHRAE. To conduct the experiments, a single cold plate-based benchtop setup was constructed, utilizing a thermal test vehicle (TTV), pump, reservoir, flow sensor, pressure sensors, thermocouple, data acquisition units, and heat exchanger. Each coolant was tested using a dedicated cold plate, and thorough cleaning procedures were carried out before each experiment. The experiments were conducted under consistent boundary conditions, with a TTV power of 1000 watts and varying coolant flow rates (ranging from 0.5 lpm to 2 lpm) and supply coolant temperatures (17°C, 25°C, 35°C, and 45°C), simulating warm water cooling. The thermal resistance (Rth) versus flow rate and pressure drop (ΔP) versus flow rate graphs were obtained for each coolant, and the impact of different supply coolant temperatures on pressure drop was characterized. The data collected from this study will be utilized to calculate the Total Cost of Ownership (TCO) in future research, providing insights into the impact of coolant selection at the data center level. There is limited research available on the reliability used in direct-to-chip liquid cooling, and there is currently no standardized methodology for testing their reliability. This study aims to fill this gap by focusing on the reliability of coolants, specifically propylene glycols at concentrations of 25%. To analyze the effectiveness of corrosion inhibitors in these coolants, a modified version of ASTM standard D1384, typically used for testing engine coolant corrosion inhibitors on metal samples in controlled laboratory settings, was employed. The setup involved immersing samples of wetted materials (copper, solder coated brass, brass, stainless steel, cast iron, and cast aluminum) in separate jars containing inhibited propylene glycol solutions from different vendors. This test will determine the reliability difference between the same inhibited solutions from different vendors.

Keywords: Data Center, Direct-to-chip liquid cooling, coolants, thermal performance, reliability

1. INTRODUCTION

Demand for high-performance data centers has increased in the past decade and cooling high-computing processors has become a major challenge. In a study by IBM [9], liquid cooling can be almost 3500 times more efficient than forced air cooling. Liquid cooling has been a promising solution as having a higher heat transfer removal coefficient than air cooling [1], and microchannel-based liquid cooling is an excellent choice for a thermal solution as it provides a high heat transfer coefficient [2][3].

Much research has been conducted to improve the cooling with a direct-to-chip liquid cooling approach, including single cold plate performance testing to rack-level testing. In a study [4], the author developed and validated approximate physics-based analytical models for the TISE, or split flow cold plates used in single-phase indirect liquid cooling. In this study, the thermo-hydraulic performance of the cold plates was investigated by conducting experiments at varying chip power, and a resistance network model was used to calculate the effective heat transfer coefficient by revealing the total resistance contributed by the elements inside the model [5]. In a CFD study, the author developed a numerical model which included the effects of inlet and outlet manifolds on the impingement microchannel cold plate hydraulic and thermal performance and with the CFD model they optimized the shape of the split flow cold plate [6-8]. In a similar study, Hadad et al. [9], performed numerical modeling of a warm water-cooled microchannel V-grooved impinged (TISE) cold plate that predicted the pressure drop and conducted the optimization, and investigated the fin tilt angle on pressure drop and thermal resistance and observed that the tilt angle had an impact on the pressure drop but the thermal resistance was a weak function for the same. A study also numerically investigated the effects of targeted coolant delivery for microchannel heatsinks and proposed a cold plate design that reduced thermal resistance by 42% [10].

In indirect liquid cooling, several research has been conducted to maximize cooling efficiency. Liquid cooling is implemented in a hybrid manner, where the cold plates are integrated in a hybrid manner, where cold plates are used to cool GPUs/CPUs and the remaining low dissipating components are cooled via air [11]. In a study, a CFD model with hybrid cooling on a 1U server was utilized to understand the heat capture ratio of the coolant and air and how the different parameters such as the inlet temperature of the air and coolant effects the heat captured by the coolant [14], an experimental investigated the effect of a new duct designed to optimize the airflow and its effects on a hybrid cooled server [25] a study showed the feasibility of rear door heat exchangers [15], In a data center, all servers work at different IT loads, at any instant time [12][13] and thus a constant flow rate could lead to excessive pumping power, thus research has been conducted on dynamic liquid cooling [16-18], a flow control device was also designed, developed and characterized to dynamically control the flow rate and increasing the pumping power savings [19-21]. At rack level, transient CFD study showed the impact of the dynamic response of the flow control device and the transient thermal and hydraulics were characterized [22]. In a study, a control strategy is shown to minimize load fluctuations in high power liquid to liquid CDUs when operated at low heat loads [23], a study also characterized different cooling loops and developed detailed analytical and numerical simulations using CFD for analyzing the entire liquid to liquid cooling which included the cooling distribution unit (CDU), they also developed a system calculator for the sizing of the secondary loop piping [24].

There have been relatively few studies that considered the effect of coolant being used. A study showed the heat transfer properties and pressure drop of different fluids and compared the coolant chemistries [26]. A study showed the corrosion mechanism for copper-based cold plates and the change in corrosion with a change in ambient conditions and captured the impact of operating conditions, that is the fluid temperature, fluid type, and galvanic potential. [27]

The liquid coolants are used in a cooling loop consisting of a cold plate, heat exchanger, and pump. The cold plate (generally made of copper) with micro-fin channels is mounted on the electronic component and captures the heat dissipated from it. There are many aqueous (water) and non-aqueous-based coolants that can be used in cooling electronic components. The general rule of using the coolant is that it must be non-flammable, economical, non-toxic, and freezing less than -40 °C and be compatible with the wetted materials that come in with coolants such as metals, and polymers, other than this the coolant must also have excellent thermos-physical properties, i.e., low viscosity, high specific heat, and thermal conductivity.

The most common coolant used in the industry is deionized water, as having very high thermal conductivity and specific heat to capture the dissipated heat, and a low viscosity helps lower the power required to pump it across the system and thus is the best cooling media, but with all the pros, because of its freezing point and expansion upon freezing make it incompatible for use in the closed loop when exposed in cold conditions due to the fear of getting the hoses burst or damage.

In order to overcome this issue, various concentrations of ethylene glycol or propylene glycol are added to reduce the freezing problem, but it also reduces the heat transfer efficiency compared to water significantly, with the addition of ethanol and methanol can make the fluid flammable as methanol is highly toxic in nature [28][29], like most metals copper also undergoes corrosion to form corrosion products [30] as it comes in contact with the coolant, thus corrosion inhibitors are added that is compatible with the coolant solution and is stable till the life of the electronics system and adequately protect the wetted metals in the cooling loop. Corrosion of the wetted components can start degrading the thermal performance and later could also lead to system failure due to fluid leakage or channel blockage in the cooling loop [31].

ASHRAE's [29] recommendations provide valuable guidance for mitigating corrosion risks in liquid cooled data centers. These recommendations include a list of wet materials that may be present in the Technology Cooling Loop (TCS) or Facility Water System (FWS) and are based on the water quality and other parameters. However, it is important to note that the corrosion process in an actual data center can vary significantly due to the fluid and thermal properties. To address this issue, several studies have recommended the use of propylene glycol and ethylene glycol of different concentrations, as these fluids have lower corrosivity and are widely considered for data center cooling. The key is to ensure the correct dilution and corrosion inhibitor, as well as a buffer to maintain the correct pH level throughout the operational life of the coolant. The Open Compute Project (OCP) recommends the use of fluids that contain propylene glycol as a freeze point depressant and an inhibitor package that is specifically designed for the metals present in the TCS loop [32]. OCP also recommends the use of an inhibitor for copper corrosion, which is a major concern in data centers. Leakage and corrosion are the two main concerns in closed-loop systems, as they can cause performance degradation or even failure in data centers. Cold plates made from aluminum or copper with coolants are particularly susceptible to galvanic corrosion, pitting corrosion, and abrasion corrosion.

To address this issue, a study was conducted to monitor the pH value and aluminum ion concentrations of the coolant in cold plates with ethylene glycol coolant [33]. The study found that pitting corrosion was the main form of corrosion in these systems. In summary, it is important to use the appropriate coolant with the correct dilution, corrosion inhibitor, and pH buffer to mitigate corrosion risks in data center cooling systems. OCP recommendations and studies provide valuable guidance in this regard, but it is important to monitor the system and adjust as needed based on the specific fluid and thermal properties in each data center.

The objective of this study is to compare and evaluate different types of single-phase liquid coolants used in direct-to-chip cold plate-based liquid cooling systems. The study aims to analyze the thermal and hydraulic performance, reliability, compatibility with wetted materials, and environmental impact of these coolants. Specifically, the study focuses on comparing the performance of the same coolant from different vendors and investigating the impact of coolant additives on thermal performance. Additionally, the study aims to fill the gap in research by examining the reliability of propylene glycol coolants at a concentration of 25% and analyzing the effectiveness of corrosion inhibitors in these coolants. The overall goal is to provide insights into coolant selection, thermal resistance, pressure drop, and reliability to optimize cooling efficiency and inform decision-making at the data center level.

2. MATERIALS AND METHODS

This chapter is divided into two main categories, first we discuss about the coolant's thermal and hydraulic testing where the thermal test vehicle, experimental setup, different coolants, cleaning procedure and methodology are discussed briefly, and in the second part briefly describes about the coolant's reliability testing using the ASTM test setup recommended in OCP guidelines.

2.1. COOLANT THERMAL AND HYDRAULIC TESTING

2.1.1. DESCRIPTION OF TTV MODULE

A thermal testing vehicle is a machine that simulates a data center server environment to assess the effectiveness of various cooling technologies. The vehicle is intended to mimic the case temperature and ambient conditions that a data center server would encounter, allowing for reliable testing and analysis of various cooling methods. To effectively imitate the conditions that a server would undergo in a real-world data center, the vehicle can be subjected to a range of various testing scenarios, such as increasing server density, higher temperatures, and varied humidity levels. This enables the evaluation of various cooling methods under a wide range of situations, providing significant insights into their effectiveness and efficiency. The thermal test vehicle used for this study is a ceramic heater of 5x5x3 cm (length x width x height) and a T-type thermocouple is grooved at the center to provide the case temperature as shown in figure 1. The bracket holds the TTV base, and the heater assembly as shown, the base holds the heater assembly which resembles a graphical processing unit (GPU) and provides the desired 1000W of heat load (Q) for testing. The cold plate is mounted over the top of this assembly and phase change thermal interface material (TIM) is used for the testing purposes.

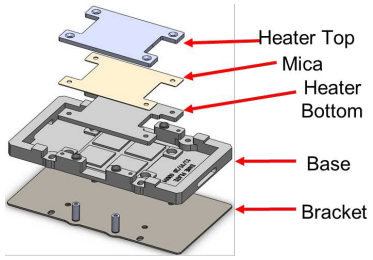

FIGURE 1: TTV DESIGN FOR COOLANT TESTING

2.1.2. EXPERIMENTAL SETUP

The thermal testing vehicle is built with a closed-loop system that includes a single micro fin channeled cold plate that serves as a direct-to-chip liquid-cooled heat sink. This cold plate is mounted on top of the thermal test vehicle, which serves as a heat source. To evaluate hydraulic and thermal properties, pressure sensors with a range of 0 to 15 psi and t-type thermocouple with a range of -185℃ to +300℃ are mounted in series before and after the cold plate. These pressure sensors have a 0.05% precision, while the t-type thermocouple has a 0.75% accuracy. A stainless-steel reservoir is linked in series to two centrifugal pumps to circulate the fluid throughout the loop. In addition, the coolant's heat is dissipated from it and kept at the required inlet temperature by a flat plate heat exchanger that is connected to a chiller unit. A needle valve is also utilized to control the flow, and a strainer with a 50-micron screen is used to filter out any dust or foreign

particles that could harm the micro-channeled fins. Connecting all the sensors to a data-acquisition unit to log the information allows for real-time data acquisition. The thermal testing vehicle's complete design provides for reliable measurement and monitoring of hydraulic and thermal parameters, as well as the capacity to modify and manage coolant flow rate and temperature. High-precision pressure sensors, t-type thermocouples, and flow sensor are used to assure reliable data capture for thermal and hydraulic analyses. Figure 2 shows the schematic layout of the experimental setup for the coolant testing. For each coolant testing, the test setup is rebuilt with new hoses and cold plate of same parameters to ensure no cross contamination among different fluids and the test setup is thoroughly cleaned before testing the coolants. The cleaning procedure for the entire test setup is further described in this paper. Figure 3 shows the experimental setup built in the lab for the testing.

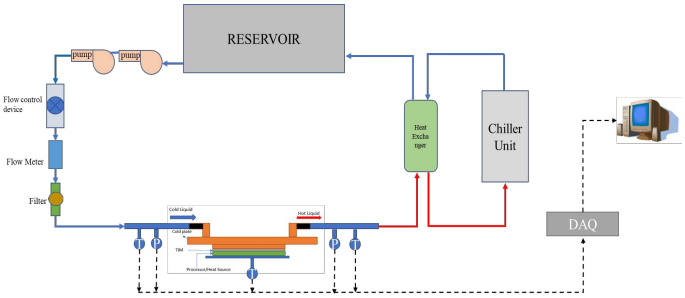

FIGURE 2: SCHEMATIC LAYOUT OF THE EXPERIMENTAL SETUP FOR COOLANT'S THERMAL AND HYDRAULIC TESTING

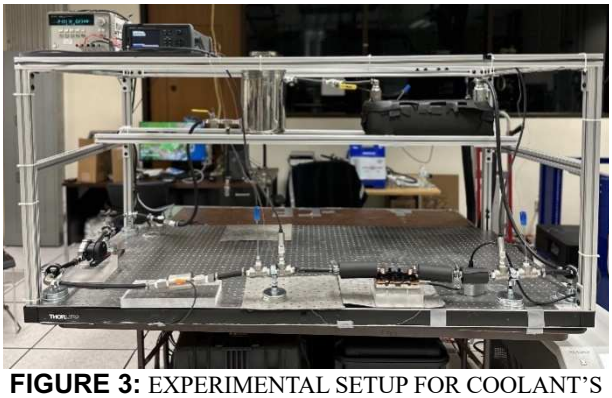

FIGURE 3: EXPERIMENTAL SETUP FOR COOLANT'S THERMAL AND HYDRAULIC TESTING

2.1.3. WETTED MATERIAL

The materials that come in direct contact with the coolant are referred to as wetted materials. The wetted materials include an EPDM rubber hose, stainless steel 316, and Copper C1100. The arrangement guarantees interoperability with the hardware in a real-time data center by utilizing these materials. Cold plates and heat exchangers frequently employ copper Cu C1100 because of its high thermal conductivity. The corrosion resistance and durability of stainless steel 316 make it ideal for usage in moist situations. Rubber EPDM hose is frequently used in fluid transfer applications because it is heat- and chemical-resistant. The fluids specification is closely tied to the wetted material list. Table 1 shows the list of wetted materials used.

Material	Details
Copper	CDA1100
Stainless Steel	304, 316 or higher grades
EPDM	Ethylene propylene diene monomer

TABLE 1: Acceptable Wetted Materials

2.1.4. UNCERTAINTY ANALYSIS

Uncertainty analysis is critical in assessing measurement accuracy and reliability for temperature, pressure, and flow sensors. Uncertainty in these sensors can be caused by a variety of variables, including random changes in measurement signals, systematic mistakes in sensor calibration, and environmental influences such as temperature, humidity, and vibration. It is critical to identify and estimate the degree of these uncertainties while undertaking uncertainty analysis. This can be performed using statistical approaches such as standard deviations or mathematical models that characterize sensor behavior and its surroundings. The overall uncertainty associated with the measurement may be estimated and displayed as a confidence interval by integrating these uncertainties using statistical models. With a particular degree of confidence, this range of values represents the predicted real value of the measured quantity. Uncertainty analysis is critical for guaranteeing measurement reliability and may be applied in scientific, industrial, and regulatory settings. It also allows for the comparison of measurement findings collected from various sensors or measurement systems, as well as the construction of traceability to national or international standards. Table 2 displays the parameters of uncertainty that were ascertained through the calibration methodologies.

Equipment	Uncertainty Values
Flow sensor	0.3%
Pressure sensor	0.25%
T-type thermocouple	± 0.75°C

TABLE 2: Uncertainty Analysis

2.1.5. CALIBRATION OF SENSORS

Pressure sensors were calibrated using the Fluke Calibration P5510 Pneumatic Comparison Test Pump, which has a dual pressure/vacuum range of 0 to 300 psi (20 bar) and 0 to 24 inHg (800 mbar). After collecting repeated pressure sensor readings, the slope and gain values were calculated to minimize data variations. The T-type thermocouples were calibrated in a Fluke Calibration 6109A Portable Calibration Bath across a temperature range of 10C to 150C. To reduce disparities between measured and real values, the slope and gain values were adjusted. The magnetic inductive flow sensor was calibrated using a Coriolis mass flow meter at varied flow rates and temperatures. Finally, the measurements were tuned

to get the appropriate span. Figure 4 shows a pneumatic pressure comparator utilized to calibrate the pressure sensos.

FIGURE 4: PNEUMATIC PRESSURE COMPARATOR

2.1.6. COOLANT DESCRIPTION

For this study, different coolants from different vendors are used for the testing, the coolants used are propylene glycol with concentrations of 10%, 25%, & 55% and ethylene glycol with concentrations of 10%, 25%, & 55%. These coolants are provided by three different vendors, namely vendor A, C and B. Among propylene and ethylene glycol, treated water is also tested and is provided from vendor N and S.

Ethylene Glycol (EG) is a common antifreeze used in automotive engine coolant; it is also used in applications including process cooling at lower temperatures. Ethylene glycol is colorless, odorless, and completely miscible with water. When inhibited with proper inhibitors it is less corrosive, but still ethylene glycol is toxic and should be handled with care. The quality of water used to make glycol solution is also important, water with low sulphate and chloride concentration (<25 ppm) is recommended. Once the inhibitors are depleted it is necessary that the old glycol is removed. And an inhibited propylene glycol (PG) possesses the same advantages as ethylene glycol of being less corrosive and in addition being non-toxic. [35] Table 3, 4 & 5 shows the different properties of EG and PG coolants from vendors A, B & C respectively. Table 6 shows the properties for treated water from vendor D and E respectively.

Vendor A		
Properties	Propylene Glycol	Ethylene Glycol
Appearance	Clear	Clear
pH	N/A	N/A
Melting Point	-60℃	-13℃
Vapor Density	N/A	N/A

Table 3: Physical & Chemical Properties for Vendor A

Vendor B	
Properties	Propylene Glycol (25%)
Appearance	Greenish Yellow
pH	7.8-8.6
Melting Point	-11.1℃
Vapor Density	Not Available

Table 5: Physical & Chemical Properties for Vendor B

Vendor C		
Properties	Propylene Glycol (10-100%)	Ethylene Glycol (15-100%)
Appearance	Clear	Clear
pH	7.0-11.0	7.0-11.0
Melting Point	-51.1℃	-16.7℃
Vapor Density	2.62	2.14

Table 4: Physical & Chemical Properties for Vendor C

Treated Water		
Properties	Vendor D	Vendor E
Appearance	Colorless	Colorless
pH	9	8.5-9.0
Boiling Point	100℃	100℃
Freeze Point	0.5℃	0.5℃

Table 6: Treated water properties from Vendor D and E

Table 7 shows the general properties at 25℃ such the thermal conductivity, viscosity, density, and specific heat capacity of the heat transfer fluids used in this study.

General Properties of Heat Transfer Fluid @ 25℃				
Fluid	Specific Heat, Cp (kJ/kg℃)	Density (kg/m^3)	Viscosity (Pa.s)	Thermal Conductivity (W/mK)
EG-10	4.0915	1022.4	0.000843	0.527
EG-25	3.8885	1041.94	0.0015	0.481
EG-55	3.395	1089.28	0.003097	0.368
PG-10	4.103	1015.80	0.0009452	0.508
PG-25	3.9675	1021.52	0.00217	0.474
PG-55	3.465	1042.72	0.006712	0.345
Treated Water	4.187	997.05	0.0008891	0.598

Table 7: Properties of Heat transfer Fluids

Table 8 shows the different concentrations of propylene glycol and ethylene glycol tested for different vendors and the type of test performed.

Coolant	Concentration (%)	Vendor	Type of Test
Propylene Glycol	10	A, &C	Thermal
	25	A, B &C	Thermal & Reliability
	55	A, & C	Thermal
Ethylene Glycol	10	A, & C	Thermal
	25	A, & C	Thermal
	55	A, & C	Thermal
Treated Water	100	D, & E	Thermal

Table 8: Concentration of PG and EG from different vendors

2.1.7. CLEANING PROCESS

The test loop was initially filled with a mixture of DI water and Spectrus NX1160 (<10 ml), an effective antibacterial agent with corrosive capabilities that is useful in concentrations ranging from 0.2 to 0.5 liters/ton. The loop was then drained and cleaned with DI water to remove any remaining cleaning solution residues. Following that, a tiny volume of coolant was injected and cycled through the loop to confirm that no traces of DI water remained that may affect the glycol concentration. After the system had been completely emptied, coolant was injected, and the reservoir was filled to the desired level. High flow rates were then employed to circulate the coolant around the loop and eliminate any air bubbles that might influence the thermal and hydraulic performance of the cold plate. Following the completion of the testing, the coolant was drained, and the cleaning procedure was repeated. To ensure that the testing results were consistent and free of cross-contamination, a fresh cold plate with the same design was used for each kind of coolant, and the EPDM hoses were replaced with new ones.

2.1.8. EXPERIMENTAL PROCEDURE

The experimental setup is constructed on a benchtop, ensuring that the loop is free from any contamination and air bubbles after following the cleaning procedure. Power is supplied to the TTV of 1000W. Before commencing the testing, the thermal interface material should settle between the heater and cold plate for maximum heat transfer. The flow rate is initially limited to a minimum at a high inlet temperature (45℃). Once the TIM is adequately set, the flow rate and inlet temperature are adjusted to the desired condition. After stable readings are obtained from the sensors, the data is logged using the data acquisition device. The study employs ASHRAE test conditions of 17℃, 25℃, 35 ℃, and 45 ℃, with flow rates maintained at 0.5lpm, 1lpm, 1.5lpm, and 2lpm for all four inlet temperatures. The entire experiment consists of 16 different scenarios performed on a single coolant, and each set of experiments is conducted for thirty minutes. The recorded inlet and outlet pressure and temperature values are then utilized to calculate the cold plate's thermal and hydraulic performance.

2.2. COLD PLATE BASED COOLANT'S RELIABILITY TESTING

2.2.1. ASTM D1384 TEST SETUP

The ASTM D1384 test setup involves the use of a 1000-mL, tall-form, spoutless beaker made of heat-resistant glass to contain the engine coolant solution and test specimens. The beaker is tightly closed with a glass lid and a rubber stopper in between to close the gaps. There are holes on the top of the glass to accommodate a water condenser, an aerator tube, and a thermometer. The temperature of the solution is measured using an ASTM Partial Immersion Temperature Measuring Instrument with a range of -20 to 150°C (0 to 302°F). A constant-temperature bath with a high-boiling liquid is used as a heater to maintain specified temperature control. Silicon 10-cSt oil is used in the thermal bath to maintain the specified temperature. The size of the bath is governed by the number of concurrent corrosion tests, and this arrangement can hold a total of six glass beakers at once. To ensure that the coolant solution is properly aerated, a gas-dispersion tube with a porosity size of 12-C is used. This tube allows for continuous aeration without plugging. The airflow meters are connected to a control know which can regulate the airflow to the aerator tube. The airflow meters are connected by blue 6mm BU tubing which can withstand up to 100psi air supply pressure from the compressor. Figure 4 shows the ASTM D1384 apparatus.

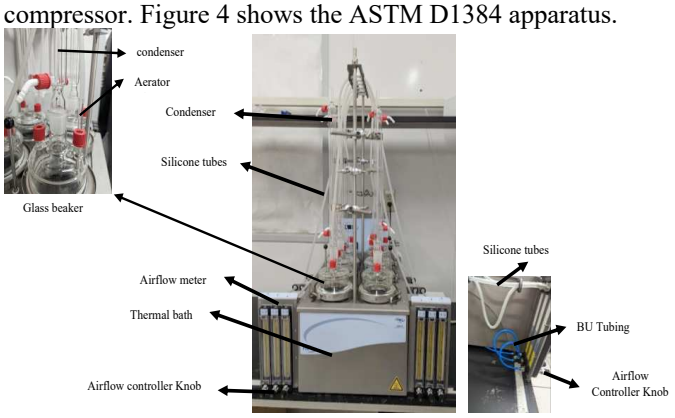

FIGURE 4: ASTM D1384 APPARATUS

2.2.2. COUPONS

The metal test specimens set comprise seven representatives of cooling system metals, and are delineated as follows.

1. Steel, UNS G10200 (SAE 1020), taken from 1.59-mm (1⁄16-in.) cold-rolled sheet stock, must be cut to a size of 50.8 by 25.4 mm (2 by 1 in.). The carbon steel's chemical composition consists of carbon (0.17 to 0.23%), manganese (0.30 to 0.60%), phosphorus (0.040% maximum), and sulfur (0.050% maximum).
2. Copper, adhering to UNS C11000 (SAE CA110)8 or UNS C11300 (SAE CA113)8, is to be cold-rolled and cut from 1.59-mm sheet stock to size 50.8 by 25.4 mm
3. Brass, conforming to Alloy UNS C26000 (SAE CA 260) must be half-hard and cut from 1.59-mm sheet stock to size 50.8 by 25.4 mm.
4. Solder - A brass specimen, should be coated with solder conforming to Alloy Grade 30A (SAE 3A) of Specification B32. Solder-coated specimens may be prepared, or used specimens can be recoated for reuse, a solid solder specimen, cut from 1.59-mm sheet stock of Alloy Grade 30A (SAE 3A) to size 50.8 by 25.4 mm, may be used subject to the mutual agreement of the parties involved. The use of a solid solder specimen must be reported along with the metal specimen weight loss results.
5. Cast Aluminum, adhering to Alloy UNS A23190 (SAE 329), should be 50.8 by 25.4 by 3.18 mm in size.
6. Cast Iron, adhering to Alloy UNS F10007 (SAE G3500), should be 50.8 by 25.4 by 3.18 mm in size.

The metal specimen arrangement must be assembled using new hardware for each test. The metal test specimens must be drilled through the center with a 6.75-mm drill to accommodate a 50.8-mm 10–24 brass machine screw covered with a thin-walled insulating sleeve of Tetrafluoroethylene tubing, with a 6.35-mm outside diameter and wall thickness of 0.4mm are

satisfactory. Two half-hard brass legs from 1.59-mm sheet stock into a size of 50.8 by 25.4 mm. Each leg should be drilled with a 6.35-mm diameter hole, centered 6.35 mm from the top and 12.7 mm from each side. The test "bundle" should be assembled on an insulated screw, with the specimens arranged in a specific order: brass leg, copper, solder, brass, steel, cast iron, cast aluminum, and brass leg. Each specimen should be separated by 4.76-mm thick solid metal spacers, having an inside diameter of 6.75 mm and an outside diameter of 11.11 mm. To insulate the brass legs and the specimen "bundle," insulating spacers made from tetrafluoroethylene should be utilized. Brass spacers should be used between the brass, solder, and copper specimens, and steel spacers between the cast iron, steel, and cast aluminum specimens. The nut should be tightened securely to guarantee a good electrical connection between the test specimens in each section of the "bundle." Figure 5 shows the coupons assembled as a bundle. Begin by scraping the cut surfaces of the cast iron and cast aluminum specimens using coarse-grade emery cloth. Eliminate any burrs on the coupon edges and holes. Employ a moistened bristle brush and ground pumice powder or fine silicon carbide grit to scour all specimens until the entire metal area is lustrous, gleaming, and devoid of any visible oxide film or tarnish. Subsequently, rinse the specimens thoroughly with tap water, followed by rinsing with acetone, drying, and weighing them up to the nearest 1 mg. Prior to recording the weight, allow the specimens to dry in a 100°C oven for 1 hour until reaching a constant weight.

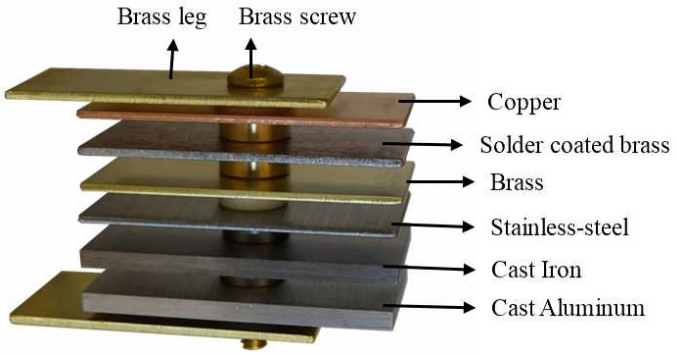

FIGURE 5: COUPON ASSEMBLY

2.2.3. CORROSIVE WATER PREPARATION

According to the ASTM D1384 standard, a solution of corrosive water is created by adding three types of salts, namely sodium sulfate, sodium chloride, and sodium bicarbonate into ultrapure water/DI water type-II. The solution is made by adding 148mg of sodium sulfate, 165mg of sodium chloride, and 138 mg of sodium bicarbonate with ultrapure to make up to 1 liter resulting corrosive water solution. To ensure precision, a predetermined amount of ultrapure water is taken in a container, and the three salts are added to it, accurately measured up to their nearest 0.1mg. A magnetic stirrer is then used to mix the salt thoroughly for 20 minutes, with a stir rod immersed in the container. This stirring process mixes the salt soluble with the ultrapure as a solvent to provide a corrosive water solution. For safety reasons, the entire process is carried out in a fume hood to avoid any spillage. Once prepared, the solution is transferred to a storage container. The pH value of the corrosive water is measured to be 8.44. Figure 6 shows corrosive water being prepared with the use of magnetic stirrer.

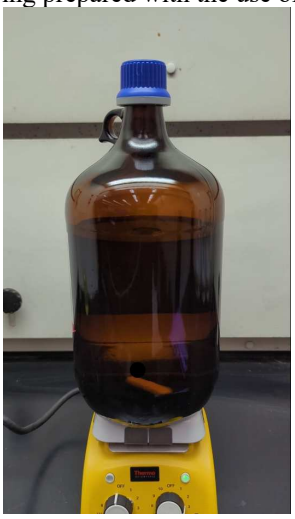

FIGURE 6: CORROSIVE WATER SOLUTION PREPARRED WITH MAGNETIC STIRRER

2.2.4. TEST SETUP

The glass jars were first cleaned to eliminate any remaining impurities, the glass jars are exposed to a rigorous cleaning procedure that includes the use of isopropyl alcohol (IPA) and deionized (DI) water. They are washed with caustic water after cleaning to remove any remnants of Deionized (DI) water and to minimize dilution inconsistencies. A properly calculated 33.33% coolant corrosive water solution is carefully poured into the glass jars. After that, the wetted materials coupon set is placed in the beaker, and the lid is tightly fastened to hold it in place throughout the test. A thermometer and an aerator tube are inserted, and the entire arrangement is sealed airtight. The individual coupon weights of each set were precisely measured, and the average weight variation is then calculated before being immersed in test beakers for each liquid. Figure 7 shows the jar with the coupon bundle immersed in coolant and corrosive water solution and the thermometer and aerator tube to provide the temperature and aeration respectively.

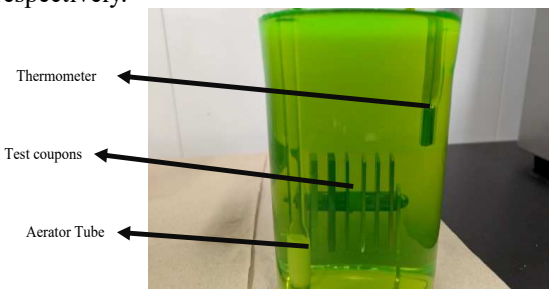

FIGURE 7: COUPON "BUNDLE" IMMERSED IN COOLANT CORROSIVE WATER SOLUTION

Figure 8 shows three jars for the same coolant to average the results.

FIGURE 8: JARS WITH COOLANT SOLUTION WITH COUPON "BUNDLE" IMMERSED

2.2.5. EXPERIMENTAL PROCEDURE

Carefully place the coupon-immersed glass beakers in the thermal bath. Adjust the silicone oil level in the bath to the appropriate level. Turn on the thermal bath and adjust the temperature to 88℃ or higher to keep the coolant corrosive water solution at 88℃ ±2℃. Start the aeration supply to the beakers and set it to 100ml/min. Check that air bubbles can be seen in all the associated beakers. Keep the chiller unit turned on and coolant circulated in the condenser tube positioned on top of the glass beaker lid. This ensures that most of the coolant condenses and does not escape as vapor. Record the weights of each coupon in the sets with 0.1 mg precision. Keep a continual eye on the temperature of the thermometers and the airflow of the device and adjust them as needed. Remove the test specimens from the beakers and place them in a desiccator after 336 hours have passed. Take samples from each beaker and thoroughly measure their pH and conductivity values. Figure 9 shows the jar placed inside the thermal bath of the ASTM apparatus which is filled with Silicon oil.

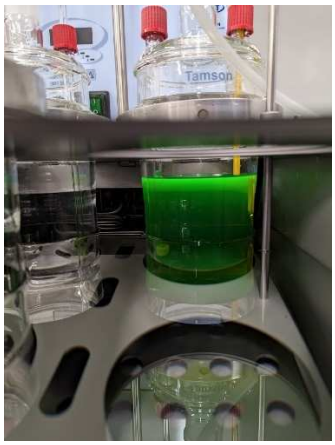

FIGURE 9: JAR PLACED IN THERMAL BATH OF ASTM D1384 APPARATUS

2.2.6. POST PROCESS

The process of cleaning involves the thorough removal of loosely adhered corrosion by-products and oxides from the surfaces of the coupon specimens. Once the coupon sets have been removed from the glass beakers, a soft bristle brush is used to meticulously clean all specimens and eliminate any remaining corrosive by-products. In the case of Iron and Steel coupons, a wet soft bristle brush is used to rinse the coupons and remove any loose corrosion products, followed using a brass scraper or bristle brush to remove adherent deposits. Finally, the coupons are scrubbed with a wet bristle brush and fine pumice to ensure complete cleaning. For Copper and Brass coupons, a 1:1 blend of concentrated HCl (density of 1.19) and water is used to eliminate tarnish coatings after which the coupons are rinsed with tap water and scrubbed with a wet bristle brush and fine pumice powder. Aluminum coupons, on the other hand, are immersed in a solution of concentrated nitric acid (HNO_3) and distilled water for 10 minutes, followed by thorough rinsing with water and a light brushing with a soft bristle brush to remove any loose films. The solder-coated brass coupon is treated by immersion in boiling 1% glacial acetic acid for 5 minutes, followed by thorough rinsing and brushing with a soft bristle brush to remove any loosened material. Figure 10 shows the coupons being immersed in the chemical solution for cleaning.

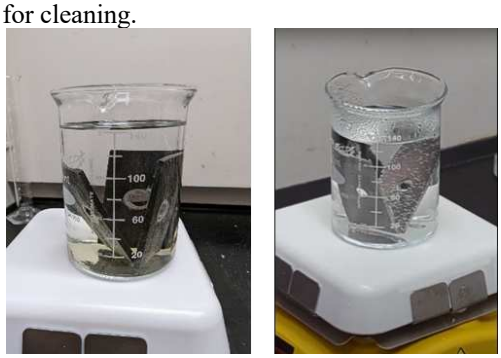

FIGURE 10: ALUMINUM COUPON IN HNO_3 (4:1) SOLUTION (LEFT), SOLDER COATED BRASS IN 1% GLACIAL ACETIC SOLUTION (RIGHT)

3. RESULTS AND DISCUSSION

The results and discussion section are broadly divided into two parts thermal & hydraulic testing and second is reliability of the secondary coolants. Cold plate-based coolants are tested at cold plate level for their thermal and hydraulic comparison using the experimental setup as shown in the previous section above. Further reliability of coolants was tested using ASTM D1384 apparatus which is the test technique for determining the corrosive effects of various coolants under stress.

3.1. THERMAL AND HYDRAULIC EXPERIMENTS

The thermal and hydraulic testing of cold plate-based coolants was performed using bench top setup as shown in the figure above. Single cold plate with TTV is used to characterize the coolants. Pump pushes the coolant from the reservoir to the cold plate extract the heat and reject it to the liquid-to-liquid heat exchanger before going back to the reservoir. The cold plate was instrumented with T type thermocouple and pressure

sensor to the inlet and outlet of it. Before starting any experimental test, the setup was cleaned following the process as explained above. All the different coolant experiments were performed at 1000 watts or 40 watts/cm² power, coolant supply temperature was varied from 17 ℃ to 45 ℃ and flow rate was varied from 0.5 lpm to 2 lpm. The coolants tested for these experiments were water-based coolants like PG with 10, 25 and 55% concentration, EG with 10, 25 and 55% concentration and treated water from multiple vendors.

3.1.1. THERMAL PERFORMANCE OF COLD PLATE BASED WATER COOLANTS

To measure the thermal performance of the coolant thermal resistance was calculated using the formula shown in below equation (1).

$$R_{th} = \frac{(T_{base} - T_{inlet})}{Q} \ (℃/W) \qquad (1)$$

Here, T_{base} is the base temperature measured from the thermocouple grooved on the heater of the TTV, and T_{inlet} is the fluid's inlet temperature, and Q is the heat load provided for testing. The graph shown below from figure 10-12 shows the thermal performance of the different concentrations of propylene glycol in the water. Figure 10 shows the PG-10 thermal resistance at different flow rates. At 0.5 lpm for vendor A coolant R_{th} was 0.04239 ℃/W and for vendor C it was 0.04119 ℃/W. At 2 lpm flow rate R_{th} for vendor A and C was dropped to 0.0226 and 0.0218 ℃/W, variation in thermal resistance value for two vendor lies within the error bar. Third bar show the average reading of the PG-10 obtained, which is 0.0417 ℃/W at 0.5 lpm and 0.0222 ℃/W at 2 lpm flow rate.

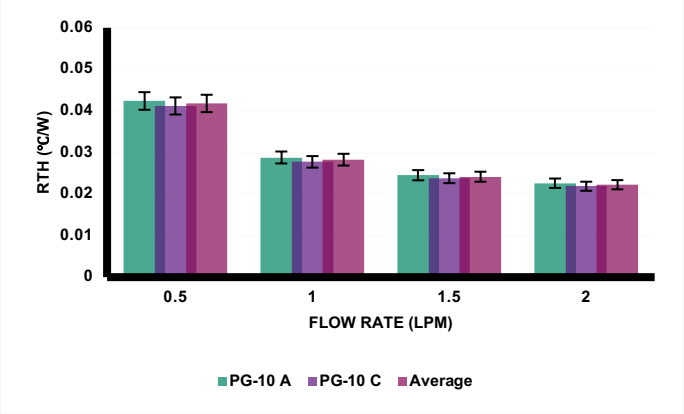

FIGURE 10: THERMAL RESISTANCE VS FLOW RATE FOR PG- 10

Figure 11 shows the PG-25 thermal resistance. For PG-25 three vendor coolants were tested, at 0.5 lpm for vendor A, B and C coolant R_{th} was observed 0.0444 ℃/W, 0.04202 ℃/W and 0.04315 ℃/W respectively. At 2 lpm R_{th} drops to 0.02419, 0.02214 and 0.02321 ℃/W respectively. The average value of R_{th} was calculated as 0.04319 ℃/W at 0.5 lpm and 0.02318 ℃/W at 2lpm. Overall, for PG-25 vendor B shows better thermal resistance than vendor A and C but it mostly lies within the error bars.

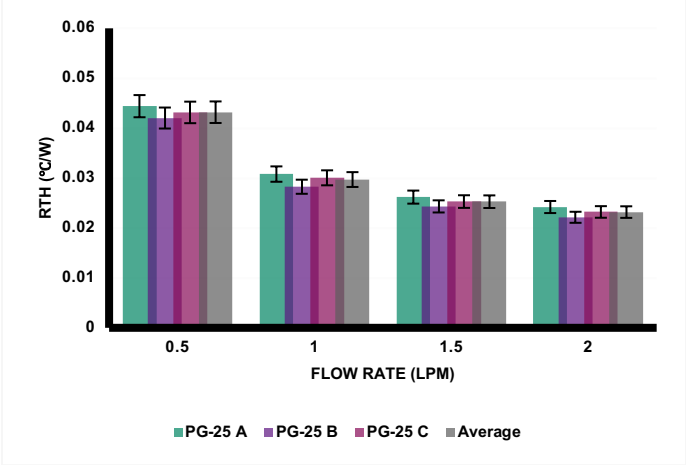

FIGURE 11: THERMAL RESISTANCE VS FLOW RATE FOR PG- 25

Similarly, Figure 12 shows the thermal resistance of the PG-55 acquired from the two different vendors. PG-55 R_{th} was observed around 0.0493 ℃/W and 0.0501 ℃/W for vendor A and C at 0.5 lpm and it dropped to 0.02707 ℃/W and 0.0284 ℃/W at 2 lpm.

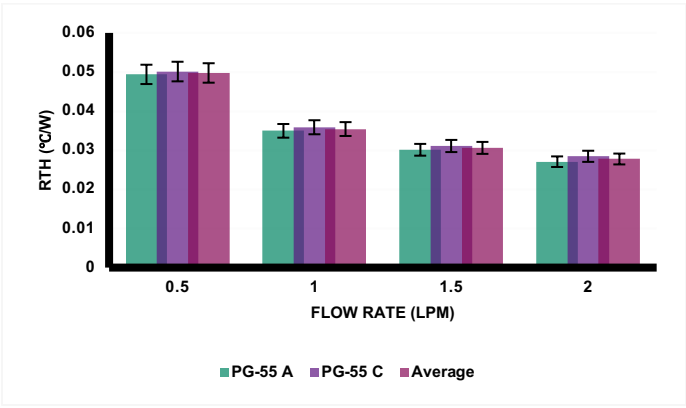

FIGURE 12: THERMAL RESISTANCE VS FLOW RATE FOR PG- 55

Overall PG-55 has shown the highest thermal resistance when compared to PG-10 and PG-25 because of its degraded thermal properties as discussed in the material and method section. PG-55 thermal performance was on an average 18.823% lower with respect to PG-25 and PG-10 show the on an average thermal performance of 4.12% higher than the PG-25.

Though PG-10 performance is better than the PG-25 and PG-55 but it is not used in the industry because of bio growth when used for long time [34]. Whereas coolants with PG concentration of more than 20% are considered biologically stable. PG-25 and PG-55 both can be used in the data centers, but PG-25 is preferred over PG-55 because of the higher thermal properties as shown.

The graph shown below from figure 13-15 shows the thermal performance of the different concentration of Ethylene glycol in the water. Figure 13 shows the EG-10 thermal resistance at different flow rates. At 0.5 lpm for vendor A and C coolant R_{th} was 0.04013 °C/W and 0.0411 °C/W. At 2 lpm flow rate R_{th} for vendor A and C was dropped to 0.0207 and 0.02111 °C/W respectively. The average reading of the EG-10 was obtained as 0.0406 °C/W at 0.5 lpm and 0.0209 °C/W at 2 lpm flow rate. Figure 14 shows the EG-25 thermal resistance. At 0.5 lpm for vendor A and C coolant R_{th} was observed 0.0418 °C/W and 0.0422 °C/W respectively. At 2 lpm R_{th} drops to 0.0223 and 0.02309 °C/W respectively. The average value of R_{th} was calculated as 0.042 °C/W at 0.5 lpm and 0.0223 °C/W at 2lpm. Figure 15 shows the thermal resistance of the EG-55 acquired from the two different vendors. EG-55 R_{th} was observed around 0.047 °C/W and 0.046 °C/W for vendor A and C at 0.5 lpm and it dropped to 0.0254 °C/W and 0.026 °C/W at 2 lpm.

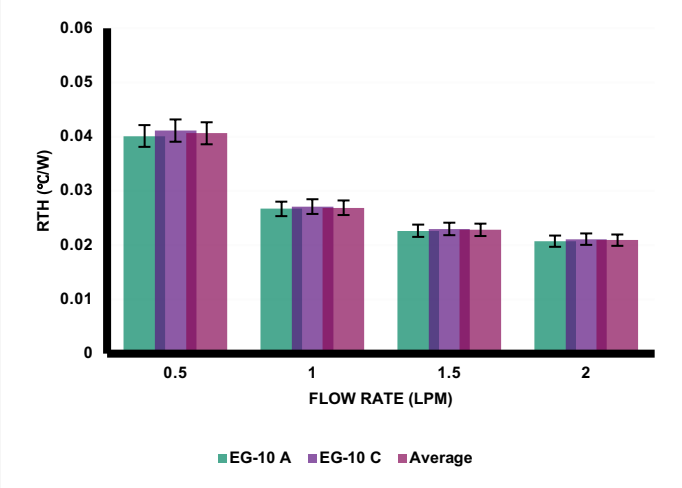

FIGURE 13: THERMAL RESISTANCE VS FLOW RATE FOR EG- 10

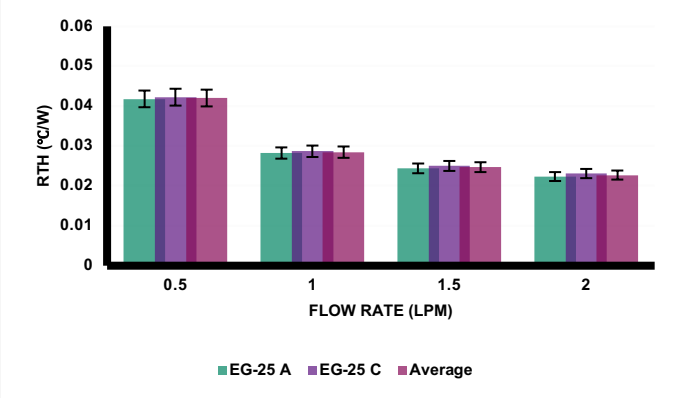

FIGURE 14: THERMAL RESISTANCE VS FLOW RATE FOR EG-25

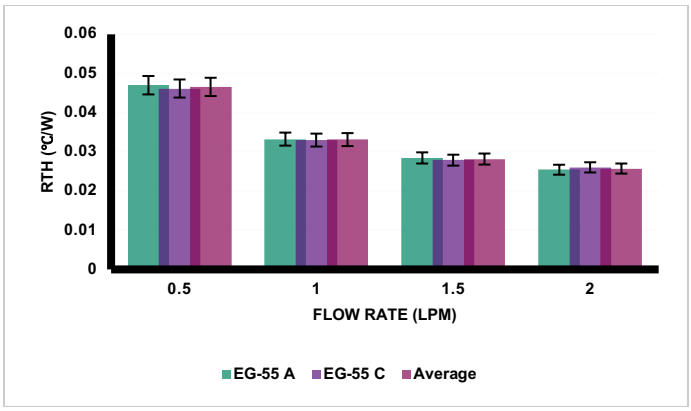

FIGURE 15: THERMAL RESISTANCE VS FLOW RATE FOR EG-55

Like PG-55 case, EG-55 has shown the highest thermal resistance when compared to EG-10 and EG-25 because of its degraded thermal properties as discussed in the material and method section. EG-55 thermal performance was on an average 10.48% lower with respect to PG-25, EG-25 show the on an average thermal performance of 2.77% higher than the PG25 and EG-10 show 8.68% higher thermal performance than PG-25. When comparing water-based coolants with ethylene glycol and propylene glycol bases, it is evident that ethylene glycol exhibits superior thermal and hydraulic performance. This can be attributed to its enhanced thermal properties, including higher thermal conductivity and viscosity, in comparison to propylene glycol-based water coolants, despite both coolants having similar thermal mass. As mentioned above in coolant description, ethylene glycol being toxic in nature is not used in data center industry.

The treated water was also tested for this study and the results of it are shown in figure 16 below. Two vendors treated water were tested and the result obtained from them are quite similar. Treated water has shown one of the lowest thermal resistances. The average value of R_{th} at 0.5 lpm and 2 lpm was obtained as 0.03906 °C/W and 0.0189 °CW respectively.

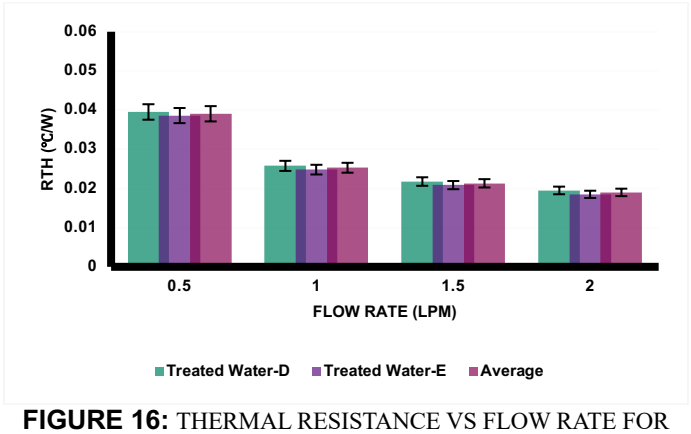

FIGURE 16: THERMAL RESISTANCE VS FLOW RATE FOR TREATED WATER

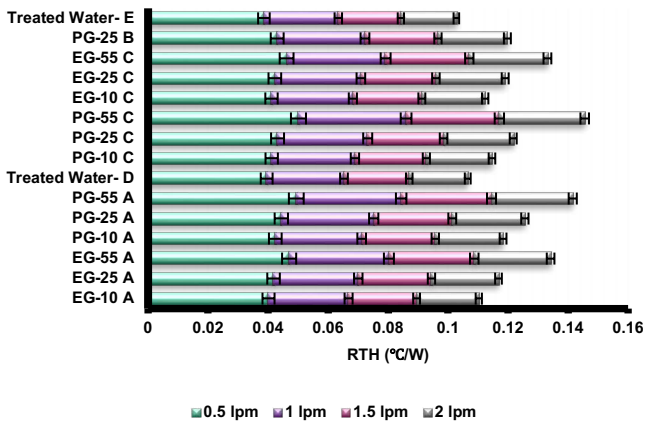

FIGURE 17: CUMMULATIVE THERMAL RESISTANCE VALUE FOR ALL COOLANTS

Figure 17 shows the cumulative thermal resistance value of all the coolants tested. It shows that treated waters have the lowest thermal resistance followed by Ethylene based coolants and followed by propylene-based coolants.

Figure 18 shows the treated water performance compared to other glycol-based coolants. The thermal performance of the treated water increases with the increase in the flow rate and concentration of glycol. The highest thermal performance of treated water is with respect to PG-55. Treated water shows 21.49% higher thermal performance at 0.5 lpm and 31.57% higher thermal performance at 2 lpm. The lowest thermal performance of treated water was with respect to EG-10, treated water thermal performance was just 3.87% higher at 0.5 lpm and 9.22% higher at 2 lpm. As compared to PG-25, which is a widely used coolant in liquid cooled data centers. Treated water performance was 9.57% higher at 0.5 lpm and 18.07% higher at 2 lpm. This higher performance of treated water will help to save pumping power at data center level. This has been discussed in the coming hydraulic testing results.

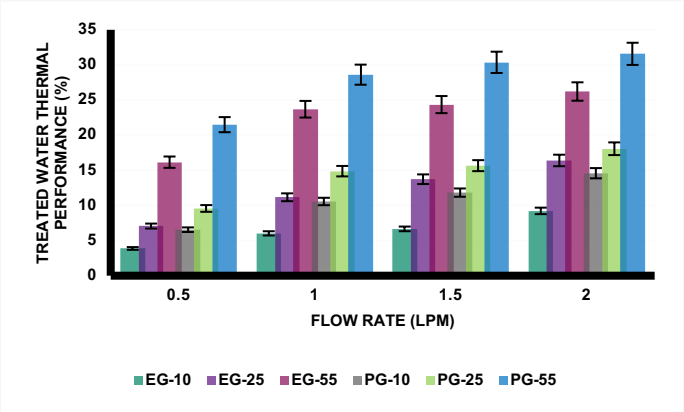

FIGURE 18: TREATED WATER PERFORMANCE COMPARED WITH OTHER GLYCOL COOLANTS

3.2. HYDRAULIC PERFORMANCE OF COLD PLATE BASED WATER COOLANTS

Liquid cooling using cold plates is an effective method for dissipating heat from electronic components. However, the pressure drop in the liquid cooling system can have a significant impact on its performance. In this study, we measured the pressure drop for different coolants at different flow rates of 0.5 lpm, 1 lpm, 1.5 lpm, and 2 lpm. The coolants used were propylene glycol (PG), ethylene glycol (EG) different concentrations (10, 25 and 55%) and treated water at four different supply temperatures (17°C, 25°C, 35°C and 45°C).

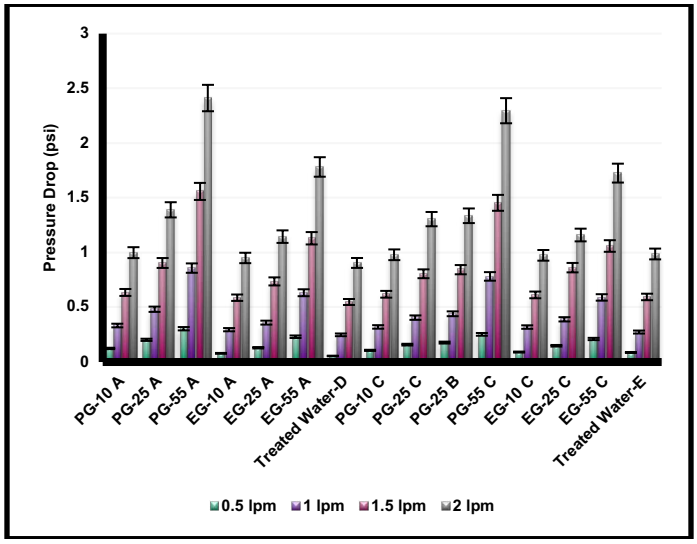

FIGURE 19: PRESSURE DROP FOR DIFFERENT COOLANTS TESTED AT DIFFERENT FLOW RATES AT 17 °C

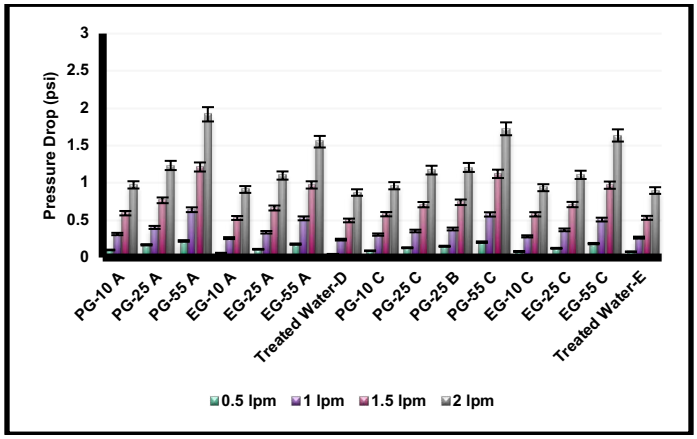

FIGURE 20: PRESSURE DROP FOR DIFFERENT COOLANTS TESTED AT DIFFERENT FLOW RATES AT 25 °C

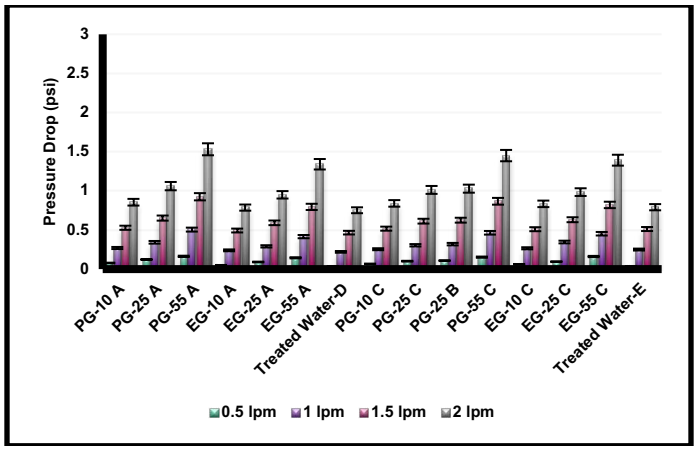

FIGURE 21: PRESSURE DROP FOR DIFFERENT COOLANTS TESTED AT DIFFERENT FLOW RATES AT 35 °C

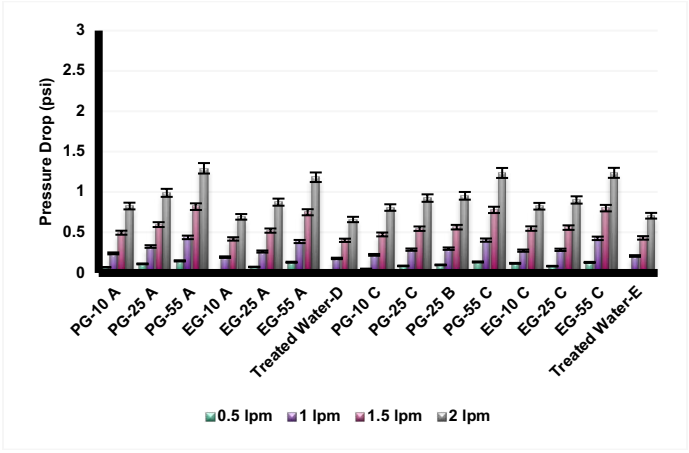

FIGURE 22: PRESSURE DROP FOR DIFFERENT COOLANTS TESTED AT DIFFERENT FLOW RATES AT 45 °C

The graph shown above from figure 19-22 shows the pressure drop of different coolants tested at different supply temperature and flow rate. Figure 19 shows the pressure drops of the all the coolants tested at 17 °C supply temperature, as expected treated water shows the lowest pressure drop as compared to other glycol-based coolants. Pressure drop of Treated water was observed to be 0.071 psi at 0.5 lpm and 0.945 psi at 2 lpm flow rate. The reason for the low pressure drops of treated water compared to other coolants is because of its lowest viscosity as shown in section 2.1.6. PG-55 has the highest pressure drop of 0.278 psi at 0.5 lpm and 2.35 psi at 2 lpm because of its highest viscosity. Similar results were obtained for the other supply coolant temperature as seen in figures 20-22. Lowest pressure drops for all the coolants were obtained at 45 °C supplied coolant temperature because for all the coolant viscosity is the function of temperature and it decreases with increase in temperature. Pressure drops of PG-55 at 45 °C were 0.142 psi and 1.26 psi at 0.5. lpm and 2 lpm respectively, whereas for treated water it was 0.0204 psi and 0.685 psi at 0.5 lpm and 2 lpm respectively.

The pressure drop in a liquid cooling system can be affected by numerous factors such as the flow rate, coolant type, coolant temperature, and the design of the cooling system. The results of this study show that the pressure drop in a cold plate-based liquid cooling system increases with increasing flow rate for all coolants tested. Moreover, the pressure drop varies depending on the coolant type and temperature. Treated water showed the lowest pressure drop, which could make it a preferred coolant for cold plate-based liquid cooling systems where low-pressure drop is desirable.

3.3. Pump Power Saving of Treated water over Other Coolants

A flow network model (FNM) has been developed with the cold plate for GPU and NV Switch connected like the arrangement in a cooling loop provided by one of the vendors. The construction of flow network model considers the length, diameter, and material properties of connecting hoses, quick disconnect pair at inlet and outlet, individual cold plates made for GPUs and NV Switches, elbows for bends and turns. A detailed description of the flow network built for the cooling loop can be found in reference [26].

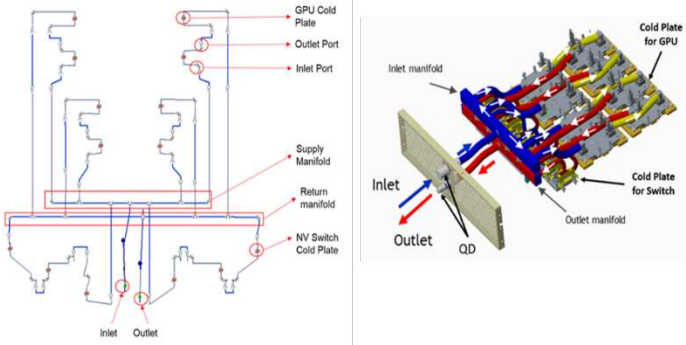

FIGURE 23: COMPONENTS IN A LIQUID COOLING LOOP AND EQUIVALENT FLOW NETWORK MODEL IN MACROFLOW

The cold plate for GPU has been tested with different coolants at various inlet temperatures. Here, we considered the coolant inlet temperature to be 35 °C and corresponding pressure drop (PQ) and thermal resistance curves (RQ) with respect to velocity has been extracted from the experimental data as shown in the previous result sections and used as input for the cold plates in flow network. For each type of coolant, the respective experimental PQ and RQ data for the cold plates with similar coolant has been used for the analysis to have precise results from the flow network model. For the cooling loop, flow rates of 6,8,9,10 LPM are considered and respective flow rates, coolant inlet and outlet temperatures for the GPU cold plate have been recorded. Previously, we had case temperature vs flow rate data for the GPU cold plate for each coolant. So, the coolant flow rate from FNM helped in determining the estimated case temperatures of GPU cold plate for each flow rate through the cooling loop. The case temperatures are then compared and flow rates per cooling loop for each coolant has been determined empirically to reach a desired case temperature 60°C. The graph displayed below

illustrates the comparative pump power savings achieved when utilizing treated water in contrast to other respective coolants. Treated water exhibits significant pump power savings, with a maximum of 95% when compared to PG-55. In the case of EG-10, treated water demonstrates a minimum pump power saving of 65%, while for PG-25, treated water exhibits a pump power saving of 75%. This data highlights the substantial energy efficiency benefits of utilizing treated water as a coolant in terms of reducing pump power requirements. While it may appear that utilizing treated water over other glycol-based coolants results in significant energy savings, conducting an analysis at the data center level reveals that these gains are comparatively small. The results of this research at data center level will be presented in future papers.

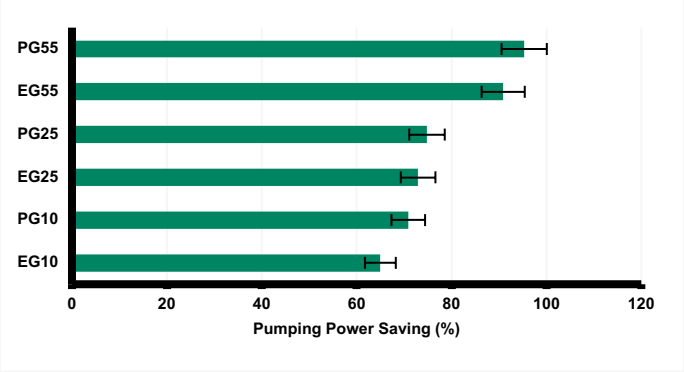

FIGURE 24: PUMPING POWER SAVINGS FOR DIFFERENT HEAT TRANSFER COOLANTS

3.4. COOLANT'S RELIABILITY

The testing procedure involved the rigorous examination of three propylene glycol (PG-25) coolants procured from vendor A, B and C. The tests were carried out at a high-temperature range of 88℃ ± 2 ℃ and a steady air supply rate of 100 ±10 ml/min over an extensive duration of 336 hours. The primary objective of these tests was to evaluate the efficacy of each coolant's inhibitors and their ability to resist the onset of corrosive reactions. As the test progressed, a visible discoloration on all three coolants was noticed. At the end of the test, the coolant from vendor B had transitioned to a brownish-green color from greenish yellow as seen in figure 26, while the initially transparent coolant A had turned into a brownish hue as seen in figure 25, the coolant from vendor C had changed to brownish color from transparent as shown in figure 27. Such alterations in appearance could indicate a potential breakdown in the coolant's chemical composition, leading to a reduction in its performance. Subsequently, a thorough analysis of the test coupons from all the coolants was conducted. It was observed that the test coupons from Vendor B coolant exhibited minimal corrosion and precipitates forming on them. In contrast, the coupon sets from Vendor A and C coolant had a higher rate of oxide formation on the surface particularly for the cast iron and Aluminum coupons, indicating a lower resistance to corrosion inhibitors and water-based coolants. The formation of oxides on the coupon surfaces can be attributed to the presence of dissolved oxygen in the coolant, which can trigger corrosive reactions. Table 9 shows the amount of weight change of the specimen before and after the test in milligrams(mg) for Vendor A, Table 10 shows for Vendor B and table 11 shows for vendor C.

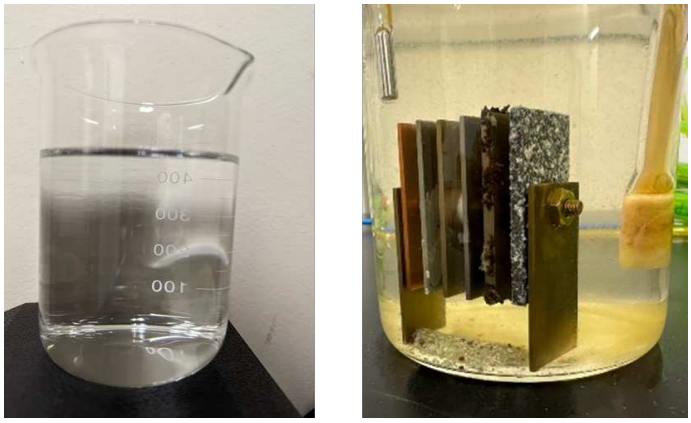

FIGURE 25: VENDOR A PG-25 COOLANT SOLUTION BEFORE TEST (LEFT) AND AFTER TEST (RIGHT)

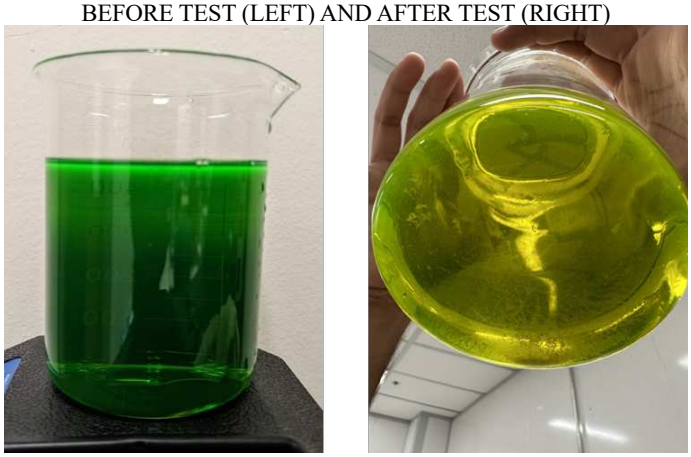

FIGURE 26: VENDOR B PG-25 COOLANT SOLUTION BEFORE TEST (LEFT) AND AFTER TEST (RIGHT)

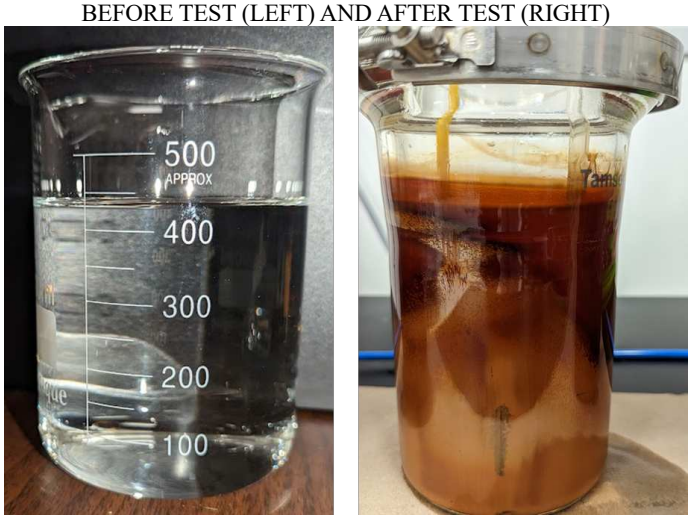

FIGURE 27: VENDOR C PG-25 COOLANT SOLUTION BEFORE TEST (LEFT) AND AFTER TEST (RIGHT)

Vendor A	Copper	Solder coated brass	Brass	Stainless steel	Cast Iron	Aluminum
Set 1	2.29	-0.83	4.75	0.32	65.97	150.2
Set 2	2.90	5.11	4.06	-0.26	94.23	174.59
Set 3	2.32	-0.58	5.63	0.36	93.91	200.01
Average	2.50	0.00123	4.81	0.14	84.7	174.93

Table 9: Change of Weight (mg) of Coupons for PG-25 from Vendor A

Vendor B	Copper	Solder coated brass	Brass	Stainless steel	Cast Iron	Aluminum
Set 1	2.99	1.5	1.71	-0.12	1.11	29.21
Set 2	1.89	1.38	1.7	-0.78	0.69	37.74
Set 3	2.26	1.61	3.44	-2	-0.82	36.74
Average	2.38	1.5	2.29	-0.96	0.33	34.52

Table 10: Change of Weight (mg) of Coupons for PG-25 from Vendor B

Vendor C	Copper	Solder coated brass	Brass	Stainless steel	Cast Iron	Aluminum
Set 1	2.16	19.62	3.69	1367.66	1093.04	49.05
Set 2	1.71	11.98	1.94	930.81	595.06	27.5
Set 3	2.39	20.47	3.01	881.97	540.03	31.98
Average	2.09	17.36	2.88	1060.15	724.71	36.18

Table 11: Change of Weight (mg) of Coupons for PG-25 from Vendor C

ASTM RECOMMED	Copper	Solder Coated Brass	Brass	Stainless Steel	Cast Iron	Aluminum
	10	30	10	10	10	30

Table 12: ASTM D 3306 Recommended Weight Loss in milligrams(mg) [36]

Based on data evaluation on the coupon sets after cleaning operations were performed, it appears that corrosion inhibitors incorporated in Vendor B PG-25 surpass those present in Vendor A and C in terms of efficacy. Specifically, the average weight loss exhibited by copper, brass, and stainless-steel coupons immersed in vendor B's PG-25 was considerably lower compared to those submerged in vendor A's PG-25. This indicates that vendor B's formulation is superior in terms of preventing corrosion, thereby ensuring better protection for metallic surfaces exposed to corrosive environments. However, it is important to note that the weight loss values for the materials copper, brass, and stainless steel were still within the recommended guidelines set forth by ASTM standards [36] shown in table 12. The negative value in the above table shows the weight gain over the test, this could be due to compound formation after the chemical reaction during the testing hours. Figure 26 shows the post image of coupon "bundle" after the test for all vendor A, B and C, it can be visually observed from the below figure that the cast aluminum and cast iron from the left of the coupon "bundle" have reacted more for Vendor A &C compared to Vendor B.

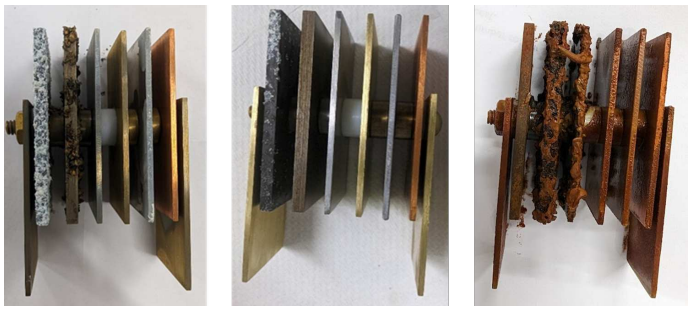

FIGURE 28: COUPON "BUNDLE" POST TEST FOR VENDOR A (LEFT), VENDOR B (CENTER) AND VENDOR C

In conclusion, the tests conducted on similar coolants from different vendors provided valuable insights into their performance under severe conditions. The discoloration observed in coolants and the varying degree of corrosion on the test coupons highlighted the importance of monitoring and maintaining the coolant systems regularly. Effective management of the coolant system can prolong the coolant's lifespan.

3.4.1. COUPON COMPARISON

We compared the metal specimen coupons immersed in PG-25 for reliability testing for different vendors. Figure 29 shows the original images of metal coupons before they were immersed in the coolant, and figures 30, 31 and 32 show the post process coupon images after the reliability test was conducted on the coolants from vendor A, B and C respectively.

FIGURE 29: METAL SPECIMEN BEFORE TESTING

FIGURE 30: METAL SPECIMEN IMMERSED IN PG-25 OF VENDOR A

FIGURE 31: METAL SPECIMEN IMMERSED IN PG-25 OF VENDOR B

FIGURE 32: METAL SPECIMEN IMMERSED IN PG-25 OF VENDOR C

A thorough visual analysis of the coupons following the post-processing step, with special attention on the copper, brass, and stainless-steel examples, reveals that there are only minor changes in their surface properties for Coolant A and Coolant B. However, in the instance of Coolant C, it is worth noting that the surface texture of the copper and brass specimens is identical, indicating equivalent degrees of deterioration. In contrast, the surface texture of the stainless-steel specimen has deteriorated noticeably. The visual inspection findings provide insight on the various impacts of coolant inhibitors on the surface qualities of the studied materials.

4. CONCLUSION

A variety of single-phase liquid coolants are available in the market, including propylene glycol (PG), ethylene glycol (EG), DI water, treated water, and nanofluids. Different manufacturers produce these coolants, incorporating a range of inhibitors and chemicals to improve their long-term effectiveness, prevent the growth of organisms, and offer corrosion protection. Nonetheless, the thermal performance of these coolants can be influenced by the additives used, even when the base coolant is identical. This study seeks to compare these coolant varieties and assess the performance of the same coolant obtained from different vendors. For the experimentation, a benchtop setup centered around a single cold plate was constructed. The setup included essential components such as a thermal test vehicle (TTV), pump, reservoir, flow sensor, pressure sensors, thermocouple, data acquisition units, and heat exchanger. To ensure accuracy, each coolant underwent testing on its dedicated cold plate, and meticulous cleaning procedures were performed before every experiment. Consistent boundary conditions were maintained throughout the experiments, with a TTV power of 1000 watts and varying coolant flow rates (ranging from 0.5 lpm to 2 lpm) as well as supply coolant temperatures (17°C, 25°C, 35°C, and 45°C) to simulate warm water cooling. This allowed for the acquisition of graphs depicting thermal resistance (R_{th}) versus flow rate and pressure drop (ΔP) versus flow rate for each coolant. Additionally, the effect of different supply coolant temperatures on pressure drop was thoroughly analyzed.

The current body of research on the reliability of direct-to-chip liquid cooling is limited, and there is a lack of standardized methodology for assessing their reliability. This study aims to bridge this gap by focusing on the reliability of coolants. To evaluate the effectiveness of corrosion inhibitors in these coolants, the ASTM standard D1384 was employed. This standard is typically used for testing engine coolant corrosion inhibitors on metal samples in controlled laboratory settings. In this study, samples of ASTM standard coupon such as copper, solder coated brass, brass, stainless steel, cast iron, and cast aluminum were immersed in separate containers containing inhibited coolant solutions from different vendors. By subjecting these materials to the test, the study seeks to determine any variations in reliability among the same inhibited solutions obtained from different vendors. In this paper, we have conducted reliability testing for the PG-25 coolant sourced from two different vendors. Overview of the paper touches on the following aspects.

1. For the thermal and hydraulic and testing of different coolants, a single cold plate benchtop setup was developed. Exacting standards of meticulous cleanliness were diligently upheld between the sequential experiments involving distinct coolants.
2. Upon analysis of the thermal and hydraulic testing results, it was observed that despite the utilization of diverse inhibitors and chemicals by different vendors to deter bio growth and corrosion within the identical base fluid, the thermal and hydraulic performance exhibited remarkable similarity. The disparities observed fell well within the acceptable margin of error, approximately 5%.
3. When comparing water-based coolants with ethylene glycol and propylene glycol bases, it is evident that ethylene glycol exhibits superior thermal and hydraulic performance. This can be attributed to its enhanced thermal properties, including higher thermal conductivity and viscosity, in comparison to propylene glycol-based water coolants, despite both coolants having similar thermal mass. The reason Propylene glycol 25% concentration is universally used in the data centers is because it is nontoxic and less harmful to the environment as compared to Ethylene based water coolants.
4. Among all the coolants tested, treated water exhibited the most exceptional thermal performance. The average thermal resistance of treated water at a flow rate of 0.5 liters per minute was approximately 0.039 °C/W, while at a flow rate of 2 liters per minute, it was approximately 0.0189 °C/W because of its better thermal properties.
5. The thermal performance of treated water improves as the flow rate increases, demonstrating its highest performance compared to PG-55. At a flow rate of 0.5

lpm, treated water exhibits a 21.49% higher thermal performance, and at a flow rate of 2 lpm, it shows a 31.57% higher thermal performance compared to PG-55. In comparison to PG-25, treated water demonstrates a 9.57% higher thermal performance at 0.5 lpm and an 18.07% higher thermal performance at 2 lpm.

6. This study aimed to assess the pressure drop characteristics of various coolants at different flow rates, namely 0.5 lpm, 1 lpm, 1.5 lpm, and 2 lpm. The coolants investigated in this study included propylene glycol (PG), ethylene glycol (EG) at different concentrations, and treated water. Additionally, the coolants were subjected to four distinct supply temperatures, namely 17°C, 25°C, 35°C, and 45°C. Through these measurements, we aimed to analyze the impact of flow rate, coolant type, concentration, and supply temperature on pressure drop, which is a critical parameter for evaluating coolant performance.
7. As expected, at a temperature of 17°C, treated water demonstrated the lowest pressure drop among all the tested coolants, outperforming the other glycol-based options. At a flow rate of 0.5 lpm, the pressure drop for treated water was measured at 0.071 psi, while at 2 lpm, it reached 0.945 psi. Conversely, PG-55 exhibited the highest pressure drop, reaching 0.278 psi at 0.5 lpm and 2.35 psi at 2 lpm. Consistent trends were observed at other supply coolant temperatures as well. Notably, the lowest pressure drops for all coolants were recorded when the coolant was supplied at 45°C. Specifically, PG-55 displayed pressure drops of 0.142 psi at 0.5 lpm and 1.26 psi at 2 lpm at this temperature, whereas treated water exhibited pressure drops of 0.0204 psi and 0.685 psi at 0.5 lpm and 2 lpm, respectively.
8. Treated water exhibits significant pump power savings, with a maximum of 95% when compared to PG-55. In the case of EG-10, treated water demonstrates a minimum pump power saving of 65%, while for PG-25, treated water exhibits a pump power saving of 75%. This data highlights the substantial energy efficiency benefits of utilizing treated water as a coolant in terms of reducing pump power requirements. While it may appear that utilizing treated water over other glycol-based coolants results in significant energy savings, conducting an analysis at the data center level reveals that these gains are comparatively small. The results of this research at data center level will be presented in future papers.
9. Corrosion inhibitors play a crucial role in mitigating material degradation. The effectiveness of corrosion inhibitors in coolant formulations can significantly impact the corrosion resistance of tested materials. Temperature and exposure time have a notable influence on corrosion behavior. Elevated temperatures and extended exposure durations can accelerate the corrosion process, leading to increased material degradation.
10. Visual inspections and weight analysis are valuable tools for assessing corrosion effects. Monitoring changes in surface topography and coupon weights can provide valuable insights into the performance of materials and coolants.
11. Based on the empirical results, it can be concluded that copper lost weight in all the coolant situations, with coolant C showing the lowest weight loss and coolant B showing the second lowest. In terms of weight reduction for the brass coupons, coolant B saw the least weight loss while coolant A saw the most. About stainless steel, coolant A produced the least amount of weight loss, whereas coolant C produced the most, exceeding the ASTM standard.

REFERENCES

[1] R. Schmidt, “Packaging of new servers-energy efficiency aspects,” in Proc. 1st Berkeley Symp. Energy Efficient Electron., Berkeley, CA, USA, Jun. 2009, pp. 1–35. [Online]. Available: https://e3s-center.berkeley.edu/wp-content/uploads/2017/07/RogerSchmidt.pdf

[2] Incropera, F., Liquid Cooling of Electronic Devices by Single-Phase Convection, John Wiley & Sons (New York, 1999), pp. 125-163.

[3] S. V. Garimella & V. Singhal (2004) Single-Phase Flow and Heat Transport and Pumping Considerations in Microchannel Heat Sinks, Heat Transfer Engineering, 25:1, 15-25, DOI: 10.1080/01457630490248241

[4] V. Torreblanca, A. Soto and D. Kulkarni, 2019, "Design and Testing of Liquid Cooled Thermal Solution for High Loading Processors," 18th IEEE Intersociety Conference on Thermal and Thermomechanical Phenomena in Electronic Systems (ITherm), Las Vegas, NV, USA, 2019, pp. 965-975. doi: 10.1109/ITHERM.2019.8757362

[5] Kisitu, Deogratius, and Alfonso Ortega. "Thermal-Hydraulic Analytical Models of Split-Flow Microchannel Liquid-Cooled Cold Plates With Flow Impingement." In International Electronic Packaging Technical Conference and Exhibition, vol. 85505, p. V001T02A015. American Society of Mechanical Engineers, 2021.

[6] Ramakrishnan, B., Hadad, Y., Alkharabsheh, S., Chiarot, P. R., and Sammakia, B. (July 12, 2019). "Thermal Analysis of Cold Plate for Direct Liquid Cooling of High Performance Servers." ASME. J. Electron. Packag. December 2019; 141(4): 041005. https://doi.org/10.1115/1.4044130.

[7] Gharaibeh, Ahmad R., Yaman M. Manaserh, Mohammad I. Tradat, Firas W. AlShatnawi, Scott N. Schiffres, and Bahgat G. Sammakia. "Using a Multi-Inlet/Outlet Manifold to Improve Heat Transfer and Flow Distribution of a Pin Fin Heat Sink." Journal of Electronic Packaging 144, no. 3 (2022): 031017.

[8] Gharaibeh, Ahmad R., Mohammad I. Tradat, Srikanth Rangarajan, Bahgat G. Sammakia, and Husam A. Alissa. "Multi-objective optimization of 3D printed liquid cooled heat sink with guide vanes for targeting hotspots in high heat flux electronics." International Journal of Heat and Mass Transfer 184 (2022): 122287.

[9] Y. Hadad, S. Rangararajan, K. Nemati, B. Ramakrishnann, R. Pejman, P. R. Chiarot, B. Sammakia,, "Performance analysis and shape optimization of a water-cooled impingement micro-channel heat sink including manifolds," International Journal of Thermal Sciences, vol. 148, no. ISSN 1290-0729, p. 106145, 2020.

[10] Y. Hadad, N. Fallahtafti, L. Choobineh , C. H. Hoang, V. Radmard, P. R. Chiarot, B. Sammakia, "Performance Analysis and Shape Optimization of an Impingement Microchannel Cold Plate," IEEE TRANSACTIONS ON COMPONENTS, PACKAGING AND MANUFACTURING TECHNOLOGY, vol. 10, no. 8, pp. 1304-1319, 2020.

[11] Shahi, Pardeep, Apurv Deshmukh, Hardik Yashwant Hurnekar, Satyam Saini, Pratik Bansode, and Dereje Agonafer. "Numerical Investigation on Effect of Target Coolant Delivery in Liquid-Cooled Microchannel Heat Sinks." Journal of Enhanced Heat Transfer 30, no. 1 (2023).

[12] Y. Fan, C. Winkel, D. Kulkarni, and W. Tian, “Analytical design methodology for liquid based cooling solution for high TDP CPUs,” in Proc. 17th IEEE Intersoc. Conf. Thermal Thermomech. Phenomena Electron. Syst. (ITherm), May 2018, pp. 582–586.

[13] Shalom Simon, V, Reddy, LS, Shahi, P, Valli, A, Saini, S, Modi, H, Bansode, P, & Agonafer, D. "CFD Analysis of Heat Capture Ratio in a Hybrid Cooled Server." Proceedings of the ASME 2022 International Technical Conference and Exhibition on Packaging and Integration of Electronic and Photonic Microsystems. ASME 2022 International Technical Conference and Exhibition on Packaging and Integration of Electronic and Photonic Microsystems. Garden Grove, California, USA. October 25–27, 2022. V001T01A013. ASME. https://doi.org/10.1115/IPACK2022-97445

[14] Modi, Himanshu, Pardeep Shahi, Lochan Sai Reddy Chinthaparthy, Gautam Gupta, Pratik Bansode, Vibin Shalom Simon, and Dereje Agonafer. "Experimental Investigation of the Impact of Improved Ducting and Chassis Re-Design of a Hybrid-Cooled Server." In International Electronic Packaging Technical Conference and Exhibition, vol. 86557, p. V001T01A019. American Society of Mechanical Engineers, 2022.

[15] Shalom Simon, Vibin, Himanshu Modi, Krishna Bhavana Sivaraju, Pratik Bansode, Satyam Saini, Pardeep Shahi, Saket Karajgikar, Veerendra Mulay, and Dereje Agonafer. "Feasibility Study of Rear Door Heat Exchanger for a High Capacity Data Center." In International Electronic Packaging Technical Conference and Exhibition, vol. 86557, p. V001T01A018. American Society of Mechanical Engineers, 2022.

[16] K. Hazelwood et al., “Applied machine learning at Facebook: A datacenter infrastructure perspective,” in Proc. IEEE Int. Symp. High Perform. Comput. Archit. (HPCA), Feb. 2018, pp. 620–629.

[17] V. K. Arghode, V. Sundaralingam, and Y. Joshi, “Airflow management in a contained cold aisle using active fan tiles for energy efficient data-center operation airflow management in a contained cold aisle using active fan tiles for energy efficient data-center,” Heat Transf. Eng., vol. 37, nos. 3–4, pp. 246–256, Oct. 2016, doi: 10.1080/01457632.2015.1051386.

[18] Allahverdyan, Armen E., Karen V. Hovhannisyan, Dominik Janzing, and Guenter Mahler. "Thermodynamic limits of dynamic cooling." Physical Review E 84, no. 4 (2011): 041109.

[19] Boucher, Timothy D., David M. Auslander, Cullen E. Bash, Clifford C. Federspiel, and Chandrakant D. Patel. "Viability of dynamic cooling control in a data center environment." Journal of electronic packaging 128, no. 2 (2006): 137-144.

[20] P. Shahi, S. Saini, P. Bansode and D. Agonafer, "A Comparative Study of Energy Savings in a Liquid-Cooled Server by Dynamic Control of Coolant Flow Rate at Server Level," in IEEE Transactions on Components, Packaging and Manufacturing Technology, vol. 11, no. 4, pp. 616-624, April 2021, doi: 10.1109/TCPMT.2021.3067045.

[21] Shahi, Pardeep, Apruv Pravin Deshmukh, Hardik Yashwant Hurnekar, Satyam Saini, Pratik Bansode, Rajesh Kasukurthy, and Dereje Agonafer. "Design, Development, and Characterization of a Flow Control Device for Dynamic Cooling of Liquid-Cooled Servers." Journal of Electronic Packaging 144, no. 4 (2022).

[22] Shahi, Pardeep, Satyam Saini, Pratik Bansode, Rajesh Kasukurthy, and Dereje Agonafer. "Experimental Study Demonstrating Pumping Power Savings at Rack Level Using Dynamic Cooling." Journal of Enhanced Heat Transfer 29, no. 6 (2022).

[23] Shahi, Pardeep, Amith Mathew, Satyam Saini, Pratik Bansode, Rajesh Kasukurthy, and Dereje Agonafer. "Assessment of Reliability Enhancement in High-Power CPUs and GPUs Using Dynamic Direct-to-Chip Liquid Cooling." Journal of Enhanced Heat Transfer 29, no. 8 (2022).

[24] Modi, H, Shahi, P, Sivakumar, A, Saini, S, Bansode, P, Shalom, V, Rachakonda, AV, Gupta, G, & Agonafer, D. "Transient CFD Analysis of Dynamic Liquid-Cooling Implementation at Rack Level." Proceedings of the ASME 2022 International Technical Conference and Exhibition on Packaging and Integration of Electronic and Photonic Microsystems. ASME 2022 International Technical Conference and Exhibition on Packaging and Integration of Electronic and Photonic Microsystems. Garden Grove, California, USA. October 25–27, 2022. V001T01A012. ASME. https://doi.org/10.1115/IPACK2022-97443

[25] Heydari, Ali, Pardeep Shahi, Vahideh Radmard, Bahareh Eslami, Uschas Chowdhury, Chandraprakash Hinge, Lochan Sai Reddy Chinthaparthy et al. "A Control Strategy for Minimizing Temperature Fluctuations in High Power Liquid to Liquid CDUs Operated at Very Low Heat Loads." In

International Electronic Packaging Technical Conference and Exhibition, vol. 86557, p. V001T01A011. American Society of Mechanical Engineers, 2022.

[26] Heydari, A, Shahi, P, Radmard, V, Eslami, B, Chowdhury, U, Saini, S, Bansode, P, Miyamura, H, Agonafer, D, & Rodriguez, J. "Liquid to Liquid Cooling for High Heat Density Liquid Cooled Data Centers." Proceedings of the ASME 2022 International Technical Conference and Exhibition on Packaging and Integration of Electronic and Photonic Microsystems. ASME 2022 International Technical Conference and Exhibition on Packaging and Integration of Electronic and Photonic Microsystems. Garden Grove, California, USA. October 25–27, 2022. V001T01A007. ASME. https://doi.org/10.1115/IPACK2022-97416

[27] S. C. Mohapatra and D. Loikits, "Advances in liquid coolant technologies for electronics cooling," Semiconductor Thermal Measurement and Management IEEE Twenty First Annual IEEE Symposium, 2005., San Jose, CA, USA, 2005, pp. 354-360, doi: 10.1109/STHERM.2005.1412204.

[28] C. -U. Kim et al., "Corrosion in Liquid Cooling Systems with Water-Based Coolant – Part 2: Corrosion Reliability Testing and Failure Model," 2020 19th IEEE Intersociety Conference on Thermal and Thermomechanical Phenomena in Electronic Systems (ITherm), Orlando, FL, USA, 2020, pp. 429-434, doi: 10.1109/ITherm45881.2020.9190565.

[29] Aittomaki, A., A. Lahti, "Potassium Formate as a Secondary Refrigerant", Int J. Refrig., Vol. 20, No 4, pp. 276-282, 1997.

[30] 2001 ASHRAE HANDBOOK FUNDAMENTALS, American Society of Heating, Refrigerating and Air-Conditioning Engineers, Inc. (Atlanta, 2001), pp. 21.1-21.13.

[31] D. A. Jones, Principles and Prevention of Corrosion, Prentice-Hall, Upper Saddle River, NJ, 1966.

[32] P. R. Roberge, Corrosion Engineering – Principles and Practice, McGraw Hill, 2008

[33] Guidelines for using propylene glycol- based heat transfer fluids in ... Accessed May 9, 2023. https://www.opencompute.org/documents/guidelines-for-using-propylene-glycol-based-heat-transfer-fluids-in-single-phase-cold-plate-based-liquid-cooled-racks-final-pdf.

[34] Hu, G., J. Yang, and X. Zheng. "Corrosion behavior of aluminum cold plate in ethylene glycol coolant." Corros. Prot. 38, no. 11 (2017): 871-876.

[35] Mohapatra, Satish C. "An overview of liquid coolants for electronics cooling." Electronics cooling 12, no. 2 (2006): 22.

[36] Kilmartin, William J., and David C. Dehm. Aqueous propylene glycol engine coolant for automotive and light duty applications. No. 930588. SAE Technical Paper, 1993.